Experimentally Coupled Thermokinetic Oscillators: Phase Death and Rhythmogenesis

K.-P. Zeyer,* M. Mangold, and E. D. Gilles

Max-Planck-Institut für Dynamik komplexer technischer Systeme, Leipziger Strasse 44, 39120 Magdeburg, Germany

Received: November 9, 2000; In Final Form: May 14, 2001

We present an experimental investigation of two coupled thermokinetic oscillators. The system is the exothermic iron-(III)-nitrate catalyzed oxidation of ethanol with hydrogen peroxide to ethanal and acetic acid. The coupling of two continuous flow stirred tank reactors (CSTRs) is performed in four different ways: via coupling of the cooling circuits, via exchange of reaction mass, and via combinations of both in equal and opposite directions. The experiments are modeled by a set of ordinary differential equations, which we have used in previous studies of the uncoupled free running system in a single CSTR. The model calculations predict three different kinds of qualitative behavior before and after the coupling. First, the qualitative behavior can remain unchanged, i.e., one gets steady states when steady states are coupled or one gets periodic oscillations when periodic oscillations are coupled. Second, oscillations can emerge when stationary states are coupled (rhythmogenesis). Third, oscillations are suppressed and change into steady states (phase death) when the coupling is activated. All these types of behavior can be verified in the experiments. Generating thermal oscillations by coupling can also lead to significant safety implications. We experimentally demonstrate a safe and an unsafe way of performing the rhythmogenesis experiment guided by our model calculations.

1. Introduction

The coupling of homogeneous nonlinear chemical systems has been investigated in many numerical and experimental studies. Using isothermal systems, experiments have been performed via mass coupling, coupling by electrical current, and by flow rate coupling. Mass coupling is achieved by placing a wall with pores of variable sizes between different reactors. The exchange of material occurs by diffusion and convection. Another way is to pump the reaction solutions between the reactors. Many interesting phenomena have been found in these investigations, such like in- and out-of-phase synchronization of the two coupled reactors, synchronization of the two oscillator frequencies at different ratios of natural numbers,[1] generation (rhythmogenesis)[2] or extinction (phase death)[3] of oscillations by the coupling, and generation of complex periodic and chaotic oscillations.[4] Further, large arrays of coupled reactors have been studied experimentally. Such systems can be used to encode simple binary patterns[5] or to study the propagation of perturbations.[6,7]

In electrical coupling, different redox potentials are used for the coupling of different subsystems.[8] This type of coupling shows similar phenomena as mass coupling. Phase patterns can be encoded experimentally when large arrays of reactors are coupled.[9]

A third way is the application of the flow rate as a coupling parameter. A concentration or potential is measured in reactor 1 and is converted to a flow rate which is given to reactor 2. Accordingly, in reactor 2 a concentration or potential is measured and is given back to reactor 1. This results in a mutual coupling between the two systems. Well-defined delay times can be introduced into the coupling easily. Using this coupling mode, for example, two stable limit cycles which coexist in the state space using the same parameters can be found (birhythmicity).[10]

Simple nonlinear thermokinetic reaction systems can show a rich variety of complex dynamical states in a CSTR without coupling. Even a first order exothermic reaction can show period-1 oscillations when the heat of reaction and the activation energy are sufficiently high. This has been investigated in many theoretical studies.[11] The system dynamics can become even more complex, exhibiting oscillatory states of higher periodicities or deterministic chaos, when a consecutive reaction scheme of two first-order reactions is studied.[12]

Because many industrial processes are exothermic and consist of many different process units we are interested to study the effects of coupling such systems. Concerning coupling of thermic systems mainly numerical studies have been done.[13−18] Kubíček et al.[13] and Svoronos, Aris, and Stephanopoulos[14] investigate CSTRs coupled in series. In these CSTRs, irreversible first order thermic reactions take place. Mankin and Hudson[16,17] investigate the forcing and coupling of a irreversible first-order exothermic reaction numerically. Forcing is performed by modulation of the cooling temperature and coupling is studied via bidirectional mass and heat exchange. They characterized quasiperiodicity and period-doubling sequences to chaos. Taylor and Kevrikidis[18] have revealed very complex bifurcation structures when two nonisothermal oscillating systems are coupled by mass exchange. Oscillations can be generated or suppressed when two autocatalytic nonisothermal model systems are coupled by mutual mass exchange.[15]

Several experimental examples of thermic oscillations exist[19] and the ethanol oxidation process is one of these reactions.[20,21] However, the experimental investigations focus on single uncoupled CSTRs. To our knowledge, no experimental results have been published about the behavior of coupled thermokinetic oscillating systems.

* To whom correspondence should be addressed.

10.1021/jp0041454 CCC: $20.00
Published on Web 07/11/2001

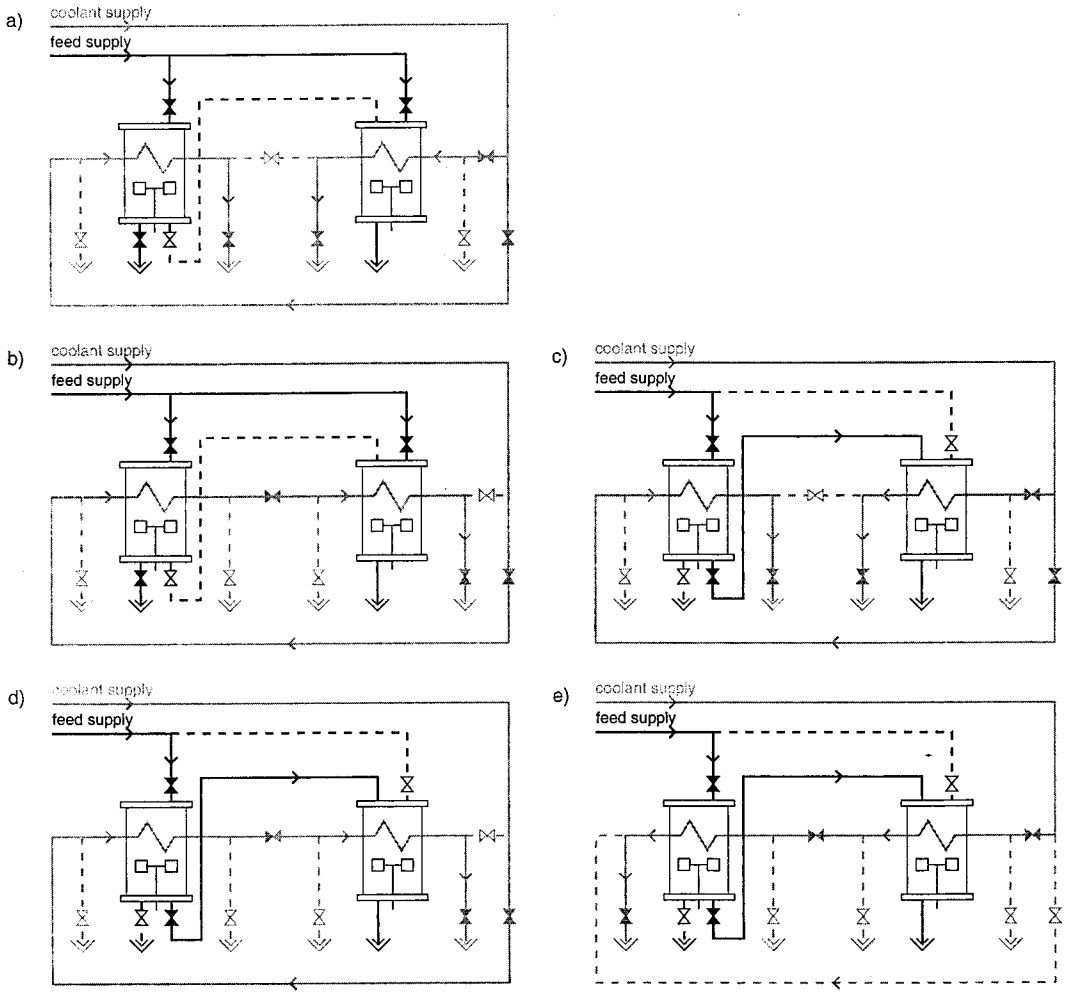

Figure 1. Schematic view of the investigated coupling situations. Black lines indicate the feed flows and gray lines mark the coolant flows. Solid lines and filled valve symbols represent active connections, whereas dashed lines and white valve symbols characterize closed connections. (a) uncoupled reactors: each reactor is fed separately with educts and each reactor has its own cooling circuit. (b) thermal coupling: the cooling circuit is connected and the coolant water enters reactor 1 (left) first and is then transferred to reactor 2 (right). The feed lines are not connected. (c) mass coupling: the feed lines are connected. The reaction mass is transferred from reactor 1 (left) to reactor 2 (right). The cooling circuits are disconnected. (d) thermal-mass coupling in equal direction: combination of the coupling situations b and c. The coolant and the reaction material enter reactor 1 first and are then transferred to reactor 2. (e) thermal-mass coupling in opposite direction: same situation as d besides that the coolant enters reactor 2 (right) first and is then transferred to reactor 1 (left).

When exothermic reactions are involved, dynamical instabilities are strongly linked with safety aspects. In the field of chemical reactor safety, it is common knowledge that not only the static stability but also the dynamic stability of exothermic reactions, which are run in a cooled CSTR, have to be evaluated.[22] Examples of direct industrial relevance which show dynamic instabilities are the oxo process[23] and many polymerization reactions.[24,25] Vleeschhouwer et al.[26] investigate autonomous thermal oscillations in an industrial oxo reactor (volume 6000 L) emphasizing safety aspects. Furthermore, the above-mentioned class of polymerization reactions, which also shows a broad spectrum of complex nonlinear dynamics such as periodic and chaotic thermal oscillations, is of great industrial importance but also has caused most of the incidents in industry.[27] Using the given criteria,[22] one should expect dynamic instabilities to occur easier when the ratio of the heat exchange surface to the reactor volume is low, which is the case in large industrial CSTRs. Although the occurrence of undesired dynamic instabilities in industrial reactors is scarcely published, there is an example of an incident in an industrial ammonia plant where temperature oscillations occurred after an undesired pressure loss.[28] To study such nonlinear phenomena in experiments, the ethanol oxidation process is chosen as it is a system which can be handled easily in the laboratory.

In this study, we investigate the coupling of two CSTRs in simulations as well as in experiments. Four different kinds of coupling are considered. The coupling scenarios are depicted in Figures 1a−e.

Thermal Coupling (Figure 1b) denotes the connection of the outlet of the coolant of reactor 1 with the inlet port of the coolant of reactor 2.

Mass Coupling (Figure 1c) signifies that the reaction mass of CSTR 1 is used as the feed stream of reactor 2 instead of fresh chemicals in the storage tanks. We also consider two combinations of these coupling modes.

Thermal-Mass Coupling in Equal Direction (Figure 1d) means that the coolant water as well as the reactants enter CSTR 1 first and are then transferred from CSTR 1 to CSTR 2.

In the case of *Thermal-Mass Coupling in Opposite Direction* (Figure 1e), the reactants enter CSTR 1 first and then are used as the feed of CSTR 2, while the coolant water enters CSTR 2 first and then flows through the cooling tube of CSTR 1.

Simulation studies are used as a guideline for experimental investigations of the coupled system. The reactor model used

TABLE 1: Reaction Enthalpies at $T = 25$ °C and $p = 101\,325.0$ Pa Used for the Model

i	$-\Delta h_R$ [kJ/mol]
1	302.5
2	385.9
3	95.1
4	0.0
5	0.0

TABLE 2: Preexponential Factors k_i and Energies of Activation E_i Used for the Model

i	k_i	E_i [kJ/mol]	ref
1	$1.494\,80 \times 10^{16}$ L mol^{-1} s^{-1}	105.50	21
2	$1.951\,32 \times 10^{20}$ L^2 mol^{-2} s^{-1}	126.20	21
3	$6.666\,00 \times 10^{14}$ L mol^{-1} s^{-1}	105.00	37
4	$1.176\,37 \times 10^{7}$ L$^{0.5}$ mol$^{-0.5}$ s^{-1}	55.69	21
5	$3.833\,30 \times 10^{4}$ s^{-1}	45.04	21

in simulations was validated by experiments at a single CSTR in previous work.[29−31] Now, the same model is used to predict the behavior of the coupled system, and to find operating conditions where the qualitative behavior of the coupled system changes. Then, the predicted behavior is verified in experiments.

2. Model System

Hafke and Gilles[20,21] experimentally demonstrated that the iron-(III)-catalyzed oxidation of ethanol with hydrogen peroxide to ethanal and acetic acid can show temperature and concentration oscillations in a CSTR. They suggested a kinetic model based on elementary steps by applying the quasi stationary state assumption to the intermediate species. The following reaction scheme was proposed[20,21]

$$CH_3CH_2OH + H_2O_2 \xrightarrow{Cat} CH_3CHO + 2H_2O \quad (1)$$

$$CH_3CHO + H_2O_2 \xrightarrow{Cat} CH_3COOH + H_2O \quad (2)$$

$$H_2O_2 \xrightarrow{Cat} 0.5\ O_2 + H_2O \quad (3)$$

$$Cat + CH_3COOH \rightarrow Cat^* \quad (4)$$

$$Cat^* \rightarrow Cat + CH_3COOH \quad (5)$$

Cat* signifies a catalytically inert acetato-iron-(III)-complex.[32] The reaction enthalpies ($-\Delta h_R$) under standard conditions ($T = 25$ °C and $p = 101\,325.0$ Pa) are compiled in Table 1. The dependence of the reaction rate constants on the temperature is described by the Arrhenius equation. The rate expressions read

$$r_1 = k_1 e^{-E_1/(RT)} c_{Cat} c_{H_2O_2} \quad (6)$$

$$r_2 = k_2 e^{-E_2/(RT)} c_{Cat} c_{H_2O_2} c_{CH_3CHO} \quad (7)$$

$$r_3 = k_3 e^{-E_3/(RT)} c_{Cat} c_{H_2O_2} \quad (8)$$

$$r_4 = k_4 e^{-E_4/(RT)} c_{Cat} \sqrt{c_{CH_3COOH}} \quad (9)$$

$$r_5 = k_5 e^{-E_5/(RT)} c_{Cat^*} \quad (10)$$

The values of the preexponential factors k_i and the energies of activation E_i are summarized in Table 2. Table 3 gives an explanation of the used symbols. The rate of reaction 6 is independent of the ethanol concentration because ethanol is in stoichiometric excess.[21]

TABLE 3: Explanations of the Used Symbols; Additional Indices 1 and 2 Refer to CSTR 1 and 2, Respectively

symbol	meaning	unit
t	time	s
T	temp	°C
p	pressure	Pa
V_L	liquid vol in the CSTR	L
$-\Delta h_R$	reaction enthalpy	kJ/mol
E_i	activation energy	kJ/mol
k_i	preexponential factor for Arrhenius equation; j: reaction order	L^{j-1}/(mol^{j-1} s^1)
r_i	reaction rate of step i	mol/(L s)
T_f	temp of the feed solution	°C
T_{cool}	temp of the coolant outlet	°C
$T_{cool,in}$	temp of the coolant inlet	°C
T_{amb}	temp of the ambient	°C
P_{heat}	heating power	W
P_{stirr}	power distributed by the stirrer	W
N_{stirr}	stirring rate	min^{-1}
w_i	weight fract. of species i	dim.less
$w_{i,f}$	weight fract. of species i in the feed	dim.less
c_i	concentration of species i	mol/L
$c_{i,f}$	concentration of species i in the feed	mol/L
n_i	no. of moles of species i	mol
ρ_f	specific density of the feed	kg/L
$c_{p,f}$	specific heat capacity of the feed	J/(K kg)
Γ	total heat capacity of the liquid reaction mixture	J/K
Γ_{ins}	total heat capacity of reactor inserts	J/K
$(UA)_{cool}$	heat transfer coeff to the coolant	W/K
$(UA)_{loss}$	heat transfer coeff to the ambient	W/K
$\dot{q}_f$	volumetric flow rate of feed	L/h
$\dot{q}_{cool}$	volumetric flow rate of coolant	L/h

To simulate the reactor behavior, the reaction scheme is implemented into a standard CSTR model.[29] The mass balances read

$$\frac{dn_{H_2O}}{dt} = \dot{q}_f(c_{H_2O,f} - c_{H_2O}) + V_L(2r_1 + r_2 + r_3) \quad (11)$$

$$\frac{dn_{H_2O_2}}{dt} = \dot{q}_f(c_{H_2O_2,f} - c_{H_2O_2}) - V_L(r_1 + r_2 + r_3) \quad (12)$$

$$\frac{dn_{CH_3CH_2OH}}{dt} = \dot{q}_f(c_{CH_3CH_2OH,f} - c_{CH_3CH_2OH}) - V_L(r_1) \quad (13)$$

$$\frac{dn_{CH_3CHO}}{dt} = \dot{q}_f(c_{CH_3CHO,f} - c_{CH_3CHO}) + V_L(r_1 - r_2) \quad (14)$$

$$\frac{dn_{CH_3COOH}}{dt} = \dot{q}_f(-c_{CH_3COOH}) + V_L(r_2 - r_4 + r_5) \quad (15)$$

$$\frac{dn_{Cat}}{dt} = \dot{q}_f(c_{Cat,f} - c_{Cat}) - V_L(r_4 - r_5) \quad (16)$$

$$\frac{dn_{Cat^*}}{dt} = \dot{q}_f(-c_{Cat^*}) + V_L(r_4 - r_5) \quad (17)$$

where V_L is the volume of the CSTR and $\dot{q}_f$ denotes the volumetric feed flow. Variables c_i and $c_{i,f}$ signify the reactor and feed concentrations of species i, respectively. The energy balance reads

$$(\Gamma + \Gamma_{ins})\frac{dT}{dt} = V_L \sum_{i=1}^{3} r_i(-\Delta h_R)_i + P_{heat} + P_{stirr} - \dot{q}_f(\rho c_p)_f(T - T_f) - (UA)_{loss}(T - T_{amb}) - (UA)_{cool}(T - T_{cool,in}) \quad (18)$$

Γ and Γ_{ins} are the total heat capacities of the liquid phase and the inserts, respectively. P_{heat} is the power introduced by the two heating elements. P_{stirr} describes the power dissipated by the stirrer. ρ_f and $c_{p,f}$ denote the density and the specific heat capacity of the feed, respectively. T, T_f, T_{amb}, and $T_{cool,in}$ are the reactor temperature, the temperature of the dosing, the ambient temperature, and the temperature of the cooling water at the inflow of the coil. $(UA)_{loss}$ and $(UA)_{cool}$ signify overall heat transfer coefficients, which describe the energy transfer to the ambient and to the cooling coil. The heat transfer coefficients on the mixture and the coolant side were calculated based on correlations from the VDI−Wärmeatlas.[33] These correlations have been optimized with a parameter identification of dynamic experiments[34] at different stirrer speeds, coolant flows, and heating powers. The heat capacity Γ_{ins} of the inserts and the overall heat transfer coefficient $(UA)_{loss}$ to the ambient were determined in the same way to be 2290 J/K and 6.6 W/K, respectively.[35] The relationship between the heat transfer coefficient to the cooling coil $(UA)_{cool}$ and the volumetric coolant flow rate $\dot{q}_{cool}$, which is the bifurcation parameter, is given in the appendices of ref 29 and 31.

This model predicts the steady-state behavior of the single CSTR and its stability characteristics accurately. It can also be used to determine the operating conditions under which the CSTR exhibits limit cycle behavior. Numerical and experimental results for different parameter sets are reported in refs 29−31.

Thermal coupling is modeled by using the outlet temperature of the coolant of reactor 1 T_{cool1} as the inlet coolant temperature of reactor 2 $T_{cool,in2}$. The volumetric coolant flow rates $\dot{q}_{cool1}$ and $\dot{q}_{cool2}$ are set equal in both reactors and density changes of the coolant water are neglected. Heat loss from the connecting tube to the ambient is also neglected. Thermal coupling is modeled by the following equations

$$T_{cool1} = T_{cool,in2} \tag{19}$$

$$\dot{q}_{cool1} = \dot{q}_{cool2} \tag{20}$$

For mass coupling, the actual composition of reactor 1 is used as the feed composition of reactor 2. The composition inside the CSTRs is described by the weight fractions $w_{i,1}$ and $w_{i,2}$, respectively, where i signifies a chemical species. The temperature of reactor 1 T_1 is used as the temperature of the feed of reactor 2 T_{f2}. Changes of the composition inside the connection tube due to chemical reactions as well as heat loss to the ambient are neglected. We use the outflow of reactor 1 directly as the feed flow of reactor 2. If oscillating conditions are present in reactor 1, the level controller of reactor 1 will give an oscillating output and accordingly an oscillating feed flow is applied to reactor 2. This agrees with the behavior of the experimental setup. For mass coupling the following equations are used

$$T_1 = T_{f2} \tag{21}$$

$$w_{H_2O_2,1} = w_{H_2O_2,f2} \tag{22}$$

$$w_{CH_3CH_2OH,1} = w_{CH_3CH_2OH,f2} \tag{23}$$

$$w_{CH_3CHO,1} = w_{CH_3CHO,f2} \tag{24}$$

$$w_{CH_3COOH,1} = w_{CH_3COOH,f2} \tag{25}$$

$$w_{Cat,1} = w_{Cat,f2} \tag{26}$$

$$w_{Cat^*,1} = w_{Cat^*,f2} \tag{27}$$

For thermal-mass coupling in equal direction, both sets of equations (eqs 19−20 and eqs 21−27) are applied. In the case of thermal-mass coupling in opposite direction, eqs 20−27 are used whereas

$$T_{cool2} = T_{cool,in1} \tag{28}$$

is used instead of eq 19.

We analyze the model numerically by integration and continuation of steady states and periodic solutions using the simulation package DIVA.[36] It is also possible to determine the stability of stationary solutions and limit cycles via calculation of the eigenvalues of the Jacobi matrix and the Floquet multipliers, respectively, using this package.

3. Experimental Setup

The experimental setup consists of two identical glass CSTRs with 3.5 liter volume each. A picture of a single reactor is given in ref 29. The reactants enter through the reactor top via two separate feed streams (water/hydrogen peroxide and water/ethanol/iron-(III)-nitrate, respectively). The feed lines are driven by piston pumps. Ethanol (96 wt %, denatured with 1 wt % methyl-ethyl ketone, Brenntag and Alkoholvertrieb Süd) and hydrogen peroxide (35 wt %, Merck) are of technical purity, whereas the iron-(III)-nitrate nonahydrate is of analytical grade (Merck). All reactant solutions are prepared with distilled water. The reactor content is permanently mixed by stirring (500 min^{-1}). The liquid volume V_L is kept constant at 2.4 L via level controllers which drive the outflow pumps. The reactors are equipped with two heating elements each. The maximum heating power for each reactor is 1600 W. Cooling is performed via cooling coils (length: 3.0 m; inside diameter: 4 mm; outside diameter: 6 mm), which are made of steel. Additionally, a reflux condenser is placed on the top of the reactors (cooling surface 0.3 m^2, gas volume inside 1.1 L, volume of the cooling water 2.21 L). The actual reactor temperatures T and the temperatures of the cooling inflows and outflows ($T_{cool,in}$ and T_{cool}) are measured by thermocouples.

For thermal coupling, both cooling lines can be connected (Figure 1b), so that the coolant outflow of reactor 1 is used as the input of the cooling of reactor 2. The length of the steel connection tube is 79 cm from reactor 1 to reactor 2 and 50 cm from reactor 2 to reactor 1. The diameter is the same as inside the reactors (see above). Mass coupling can be accomplished by feeding reactor 2 with the outflow of reactants of reactor 1 (Figure 1c). A Teflon tube of 157 cm length and 6 mm diameter is used for the connection of both reactors. These types of couplings can be investigated separately or combined. At the beginning of each experiment, both reactors are filled with 2.4 L of an aqueous solution containing ethanol and iron-(III)-nitrate nonahydrate (weight fractions 0.10 and 0.02, respectively). The coolant flows are adjusted and the heating power as well as the stirrers are turned on in both reactors. After stationary conditions have been established, the feed flow is activated for both reactors while the coupling is switched off. When both uncoupled CSTRs display stable conditions (stable steady states or stable periodic oscillations), the coupling is activated.

4. The Single System

4.1. Model Calculations. To understand the dynamics of the coupled system, it is necessary to report briefly some results for the single reactor which were obtained in previous studies.[29−31]

Figure 2 shows a typical bifurcation diagram obtained by continuation of stationary and periodic solutions. The coolant

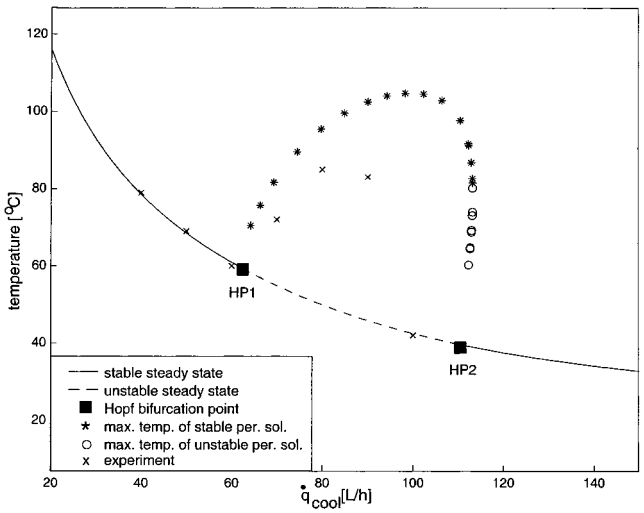

Figure 2. Model calculations of free-running system. The temperature T is plotted vs the coolant flow rate $\dot{q}_{cool}$. Conditions: weight fractions in feed: $w_{H_2O_2,f} = 0.09$, $w_{CH_3CH_2OH,f} = 0.10$, $w_{Cat,f} = 0.02$; other conditions: $V_L = 2.4$ L, $T_f = 25.0$ °C, $T_{cool,in} = 8.0$ °C, $T_{amb} = 25.0$ °C, $N_{stirr} = 500$ min^{-1}, $P_{heat} = 1600$ W, $\dot{q}_f = 5.93$ L/h.

flow rate is used as a bifurcation parameter because the reaction is very sensitive to it. At low coolant flows, the conversion of ethanol and hydrogen peroxide is high and a high yield of acetic acid can be found. In contrast, at high coolant flow rates, both conversions are low so that high amounts of hydrogen peroxide and ethanol accumulate in the reactor. A region of periodic solutions is traversed when the coolant flow $\dot{q}_{cool}$ is increased. An important result is the existence of a supercritical and a subcritical Hopf bifurcation point at the respective coolant flow rates $\dot{q}_{cool} = 61.98$ L/h and $\dot{q}_{cool} = 110.13$ L/h for the parameter set given in the figure caption. The periodic oscillations near the supercritical Hopf point show small temperature amplitudes (soft generation of limit cycles). Therefore, passing this Hopf bifurcation by increasing the coolant flow is a safe way to enter the region of periodic oscillations. In contrast, the transition from steady states at high coolant flow rates to the region of periodic solutions by reducing the coolant flow and passing the subcritical Hopf point will lead to a sudden onset of periodic solutions with high temperature amplitudes. The accumulated educts react away suddenly in a strongly exothermic reaction, which is a potential source of danger and therefore hazardous.

As starting conditions for coupling, we either choose a high-temperature steady state, a low-temperature steady state, or an oscillatory state, respectively. These starting conditions are combined with the four coupling types described above.

4.2. Experimental Results. Experimentally determined temperatures are given additionally in Figure 2. At low coolant flow rates $\dot{q}_{cool}$, the reaction displays steady states at high temperatures with low peroxide concentrations. Increasing the coolant flow rate reduces the temperature of the steady states. At $\dot{q}_{cool} = 60$ L/h, damped oscillations are observed but the system remains on a steady state. A Hopf bifurcation is crossed and stable oscillations of period-1 emerge at $\dot{q}_{cool} = 70$L/h. The amplitudes and periods of these oscillations increase when the coolant flow rate is further increased. At high coolant flow rates above $\dot{q}_{cool} = 90$ L/h, the oscillations vanish and give way to stationary solutions with low temperatures and high peroxide concentrations.

5. The Coupled System

The model calculations are performed in order to find operation conditions for subsequent experiments. After doing

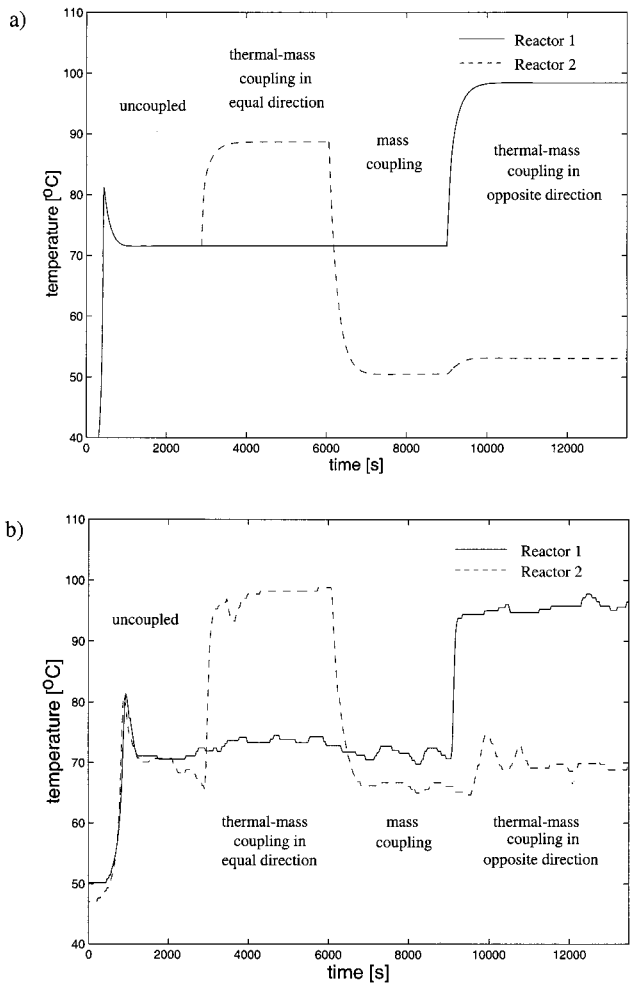

Figure 3. (a) Model calculations: coupling of high-temperature steady states; initial conditions (weight fractions) before feed flow is turned on: $w_{CH_3CH_2OH} = 0.10$, $w_{Cat} = 0.02$; other conditions: $V_L = 2.4$ L, $T_{f1,2} = 24$ °C, $T_{cool,in1,2} = 12$ °C, $T_{amb1,2} = 25$ °C, $P_{heat1,2} = 1600$ W, $N_{stirr1,2} = 500$ min^{-1}, $w_{H_2O_2,f1,2} = 0.095$, $w_{CH_3CH_2OH,f1,2} = 0.10$, $w_{Cat,f1,2} = 0.02$, $\dot{q}_{f1,2} = 5.93$ L/h, $\dot{q}_{cool1,2} = 52$ L/h; $t = 0-2881$ s: uncoupled; t = 2881−6061 s: thermal-mass coupling in equal direction; t = 6061−9001 s: mass coupling; $t = 9001-13500$ s: thermal-mass coupling in opposite direction. (b) Experimental coupling of high-temperature steady states; same conditions as in (a), except for: $\dot{q}_{cool1} = 40$ L/h and $\dot{q}_{cool2} = 38$ L/h.

the experiments, the values of the many parameters, which are recorded during the experiments and given in the respective figure captions, are used for refined calculations. These parameter sets differ a little bit for each experiment due to changes of the temperature of the cooling water or varying temperatures of the ambient on different days. Note that the coolant flows are the only parameters which have to be adjusted to the experimental results. This is necessary because heat exchange between coolant and reactor is an uncertainty in our type of model which is difficult to predict. Only the refined calculations, which are performed with the experimentally recorded parameters, are given.

5.1. Model Calculations. *5.1.1. Coupling of High-Temperature Steady States.* Figure 3a shows model calculations for coupling high-temperature steady states. Steady states at $T_{1,2} = 71.6$ °C are found. Starting from these steady states, we calculate thermal-mass coupling in equal direction, pure mass-coupling, and thermal-mass coupling in opposite direction. Thermal-mass coupling in equal direction causes reactor 2 to change to another steady state at $T_2 = 88.7$ °C. Mass-coupling results in a

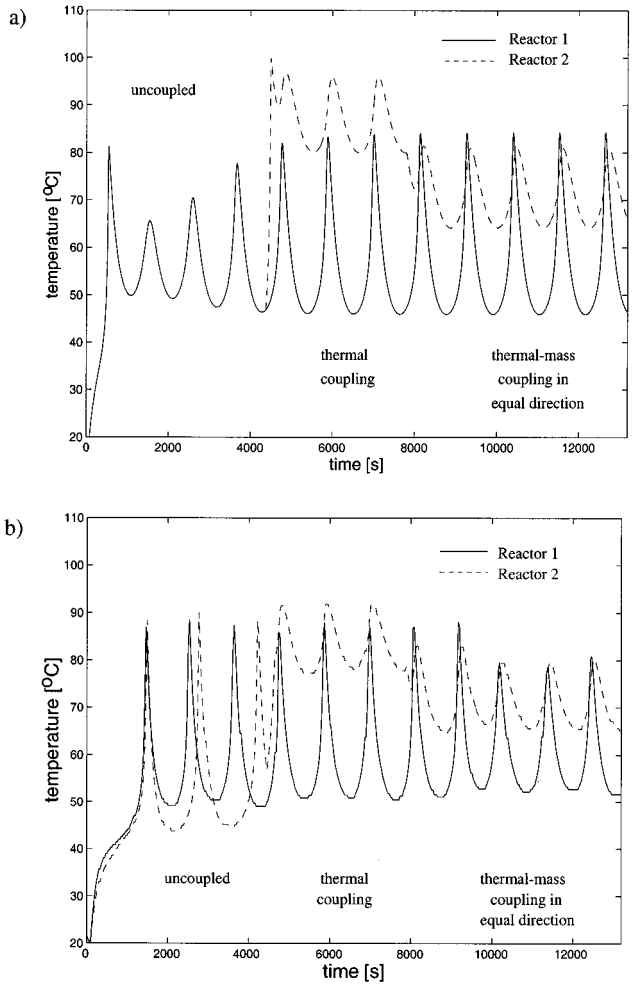

Figure 4. (a) Model calculations: coupling of oscillatory states (thermal coupling and thermal-mass coupling in equal direction); initial conditions (weight fractions) before feed flow is turned on: $w_{CH_3CH_2OH} = 0.10$, $w_{Cat} = 0.02$; conditions: $V_L = 2.4$ L, $T_{f1,2} = 19$ °C, $T_{cool,in1,2} = 11$ °C, $T_{amb1,2} = 24$ °C, $P_{heat1,2} = 1600$ W, $N_{stirr1,2} = 500$ min^{-1}, $w_{H_2O_2,f1,2} = 0.095$, $w_{CH_3CH_2OH,f1,2} = 0.10$, $w_{Cat,f1,2} = 0.02$, $\dot{q}_{f1,2} = 5.93$ L/h, $\dot{q}_{cool1,2} = 75$ L/h; $t = 0-4380$ s: uncoupled; $t = 4380-7800$ s: thermal coupling; $t = 7800-13200$ s: thermal-mass coupling in equal direction. (b) Experimental coupling of oscillatory states (thermal coupling and thermal-mass coupling in equal direction); same conditions as in Figure 4a, except for: $\dot{q}_{f1,2} = 5.93$ L/h, $\dot{q}_{cool1} = 70$ L/h, and $\dot{q}_{cool2} = 65$ L/h.

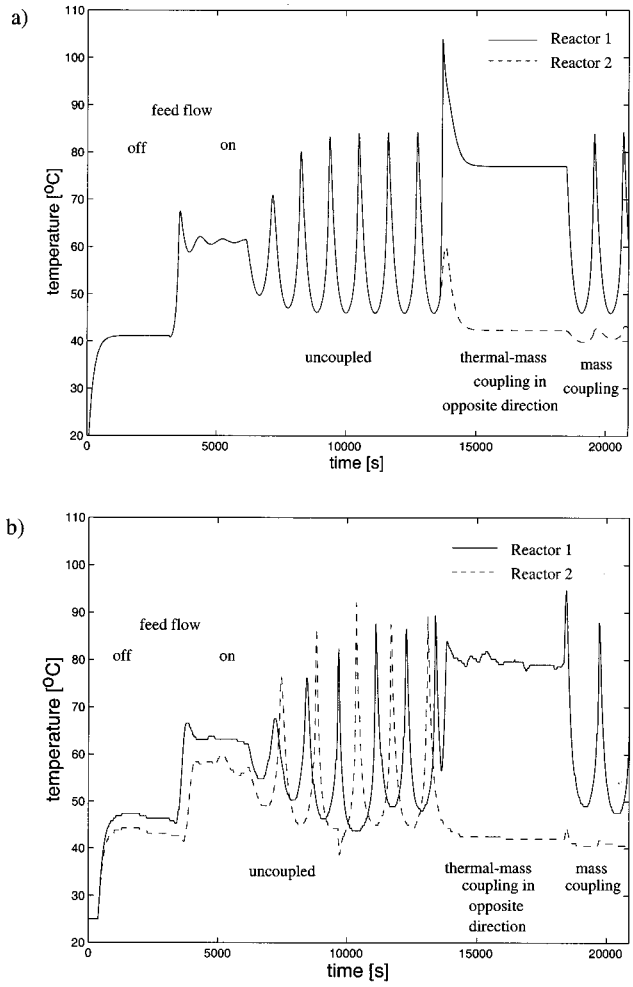

Figure 5. (a) Model calculations: coupling of oscillatory states (thermal-mass coupling in opposite direction and mass coupling); initial conditions (weight fractions) before feed flow is turned on: $w_{CH_3CH_2OH} = 0.10$, $w_{Cat} = 0.02$; conditions: $V_L = 2.4$ L, $T_{f1,2} = 19$ °C, $T_{cool,in1,2} = 11$ °C, $T_{amb1,2} = 24$ °C, $P_{heat1,2} = 1600$ W, $N_{stirr1,2} = 500$ min^{-1}, $w_{H_2O_2,f1,2} = 0.095$, $w_{CH_3CH_2OH,f1,2} = 0.10$, $w_{Cat,f1,2} = 0.02$, $t = 0-3180$ s: $\dot{q}_{f1,2} = 0$, $t = 3180-20881$ s: $\dot{q}_{f1,2} = 5.93$ L/h; $t = 0-6150$ s: $\dot{q}_{cool1,2} = 65$ L/h; $t = 6150-20881$ s: $\dot{q}_{cool1,2} = 75$ L/h; $t = 0-13620$ s: uncoupled; t = 13 620−18480 s: thermal-mass coupling in opposite direction; t = 18 480−20 881 s: mass coupling. (b) Experimental coupling of oscillatory states (thermal-mass coupling in opposite direction and mass coupling); same conditions as in Figure 5a, except for: $t = 0-6150$ s: $\dot{q}_{cool1} = 58$ L/h and $\dot{q}_{cool2} = 56$ L/h; $t = 6150$ s − 20881 s: $\dot{q}_{cool1} = 72$ L/h and $\dot{q}_{cool2} = 61$ L/h.

temperature decrease of reactor 2 of about 21.1 °C compared with the uncoupled steady state. When thermal-mass coupling in opposite direction is investigated, the temperature in reactor 1 increases strongly because the higher coolant temperature leads to much higher conversions. Reactor 1 adopts a steady state at $T_1 = 98.4$ °C. At the same time, the temperature in reactor 2 is much less affected, because conversion remains low. Reactor 2 shows a steady state with low conversion at $T_2 = 53.1$ °C.

5.1.2. Coupling of Oscillatory States. In Figures 4a and 5a, we present the calculations referring to the experimental runs in Figures 4b and 5b. For these calculations, we set the coolant flow rate to $\dot{q}_{cool1,2} = 75$ L/h in both reactors to have a situation comparable with the corresponding experiments for the uncoupled system. Oscillations of period 1 are found using this parameter set. Thermal coupling decreases the amplitudes of the period-1 oscillations in reactor 2, whereas the temperature average of the oscillations is increased (Figure 4a). Reactor 1 remains unchanged because it is not influenced by this coupling mode. Thermal-mass coupling in equal direction results in period-1 oscillations of similar amplitudes as in the case of thermal coupling but the average temperature is decreased (Figure 4a). Thermal-mass coupling in opposite direction causes the oscillations in both reactors to vanish and to give way to steady states. This phenomenon, known as phase death, seems to be interesting for technical applications. Obviously, the thermal-mass coupling in opposite direction can be used to stabilize reactors whose steady states would be unstable under the same conditions in the uncoupled case. Reactor 1 changes to a high-temperature steady state at $T_1 = 77.0$ °C, whereas reactor 2 shows a low-temperature steady state at $T_2 = 42.3$ °C (Figure 5a). When pure mass-coupling is investigated reactor 2 shows very small temperature oscillations with an amplitude of about 2.6 °C (Figure 5a).

5.1.3. Coupling of Low-Temperature Steady States. Finally, we investigate the coupling of low-temperature steady states. We use $\dot{q}_{cool1} = 130$ L/h and $\dot{q}_{cool2} = 125$ L/h as coolant flow

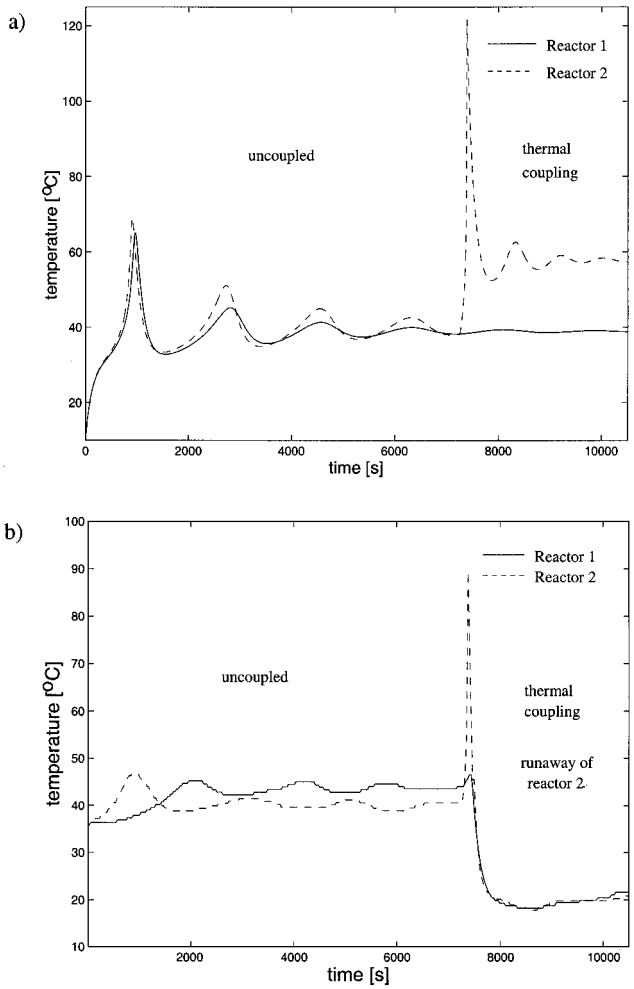

Figure 6. (a) Model calculations: coupling of low-temperature steady states; initial conditions (weight fractions) before feed flow is turned on: $w_{CH_3CH_2OH} = 0.10$, $w_{Cat} = 0.02$; conditions: $V_L = 2.4$ L, $T_{f1,2} = 23$ °C, $T_{cool,in1,2} = 11$ °C, $T_{amb1,2} = 24$ °C, $P_{heat1,2} = 1600$ W, $N_{stirr1,2} = 500$ min^{-1}, $w_{H_2O_2,f1,2} = 0.090$, $w_{CH_3CH_2OH,f1,2} = 0.10$, $w_{Cat,f1,2} = 0.02$, $\dot{q}_{f1,2} = 5.93$ L/h, $\dot{q}_{cool1} = 130$ L/h, $\dot{q}_{cool2} = 125$ L/h; $t = 0-7260$ s: uncoupled; $t = 7260-10515$ s: thermal coupling; the sharp temperature increase up to $T = 119.2$ °C in reactor 2 indicates a thermal runaway after the coupling in activated. (b) Experimental coupling of low-temperature steady states; same conditions as in Figure 6a, except for: $\dot{q}_{cool1} = 132$ L/h and $\dot{q}_{cool2} = 125$ L/h; a thermal runaway of reactor 2 occurs after thermal coupling is activated.

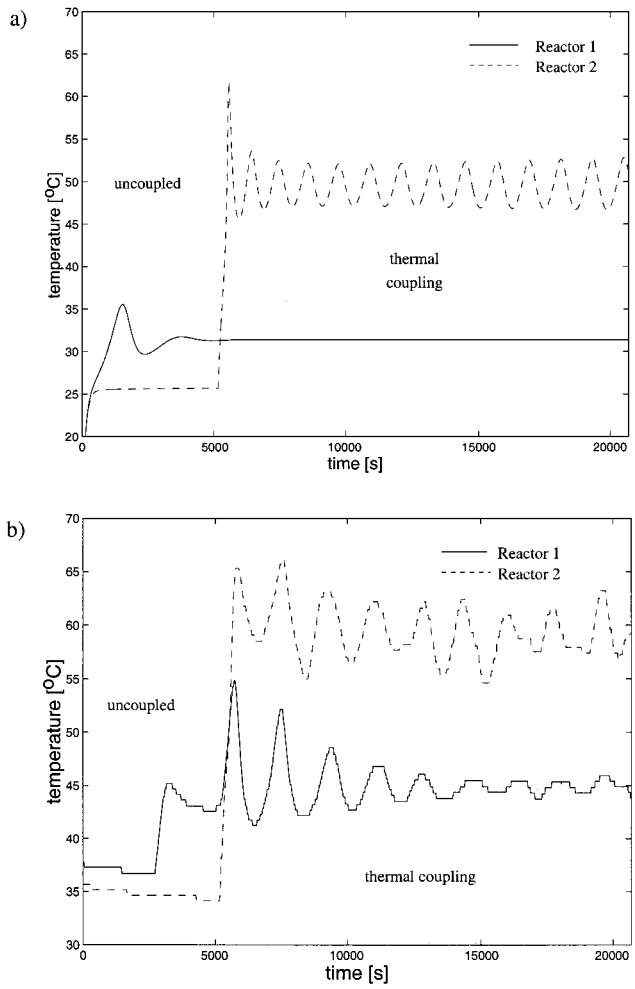

Figure 7. (a) Model calculations: coupling of low-temperature steady states; initial conditions (weight fractions) before feed flow is turned on: $w_{CH_3CH_2OH} = 0.10$, $w_{Cat} = 0.02$; conditions: $V_L = 2.4$ L, $T_{f1,2} = 20$ °C, $T_{cool,in1,2} = 6$ °C, $T_{amb1,2} = 21$ °C, $P_{heat1,2} = 1600$ W, $N_{stirr1,2} = 500$ min^{-1}, $w_{H_2O_2,f1} = 0.095$ and $w_{H_2O_2,f2} = 0.0$ before coupling, $w_{H_2O_2,f1,2} = 0.095$ after coupling, $w_{CH_3CH_2OH,f1} = 0.10$ and $w_{CH_3CH_2OH,f2} = 0.179$ before coupling, $w_{CH_3CH_2OH,f1,2} = 0.10$ after coupling, $w_{Cat,f1} = 0.02$ and $w_{Cat,f2} = 0.034$ before coupling, $w_{Cat,f1,2} = 0.02$ after coupling, $\dot{q}_{f1} = 5.93$ L/h and $\dot{q}_{f2} = 3.64$ L/h before coupling ($t = 0-5160$ s), $\dot{q}_{f1,2} = 5.93$ L/h after coupling ($t = 5160-20700$ s), $\dot{q}_{cool1,2} = 138$ L/h; $t = 0-5160$ s: uncoupled; $t = 5160-20\,700$ s: thermal coupling; a safe coupling procedure is predicted when the hydrogen peroxide flow is activated not before the thermal coupling starts. The temperature peak after the thermal coupling is diminished from $T = 119.2$ °C in Figure 6a to $T = 61.8$ °C. (b) Experimental coupling of low-temperature steady states; same conditions as in Figure 7a, except for: $\dot{q}_{cool1} = 138$ L/h and $\dot{q}_{cool2} = 122$ L/h; safe coupling procedure: the hydrogen peroxide feed of reactor 2 is activated not before the thermal coupling is turned on.

rates for the model calculations. Figure 6a shows the result for thermal coupling. The coupling causes reactor 2 to change from a steady state at $T_2 = 39.8$ °C to another steady state at $T_2 = 57.8$ °C. This temperature is far below the boiling point of the reaction mixture (~100 °C) and does not seem to cause any problems for safe reactor performance. The transient phase, however, shows a sharp temperature peak with a maximum at $T_2 = 119.2$ °C. This fast temperature rise is associated with a strong evolution of oxygen. This indicates a thermal runaway when an experiment is carried out under these conditions. As a guideline for the experiment in Figure 7b, where the thermal coupling is performed in a safe manner, we test to switch on the hydrogen peroxide feed not before the moment of coupling so that its accumulation is prevented. We further increase the amount of hydrogen peroxide in the feed from $w_{H_2O_2,f1,2} = 0.090$ to $w_{H_2O_2,f1,2} = 0.095$. Figure 7a shows the model calculation, which strongly resembles the experiment in Figure 7b. The temperature peak at the beginning of the coupling is reduced from $T_2 = 119.2$ °C to $T_2 = 61.8$ °C although more hydrogen peroxide is contained in the feed. In contrast to Figure 6a, oscillations are now generated by the coupling. This means that the coupling of two reactors might also have a destabilizing effect on the system. This behavior, known as rhythmogenesis, is often undesirable in technical applications and must be accounted for in process design.

5.2. Experimental Results. *5.2.1. Coupling of High-Temperature Steady States.* The simulation results for the coupled system are used as a guideline for performing the experiments. First, we investigate the coupling of high-temperature steady states ($T_{1,2} \approx 70$ °C). Figure 3b shows an experimental run where different types of coupling are investigated. One can recognize that the thermal-mass coupling in equal direction

causes reactor 2 to switch to another steady state with higher temperature which agrees qualitatively with the simulation results ($T_2 = 98$ °C, model: $T_2 = 88.7$ °C). When the thermal coupling is switched off and only the mass transfer remains activated, the temperature of reactor 2 drops down to $T_2 = 66$ °C, which is about 4 °C below the corresponding temperature of the steady state before coupling ($T_2 = 70$ °C). In the model calculations, we find a significantly larger temperature decrease of 21.1 °C (see chapter 5.1.1 and Figure 3a). Reactor 1 shows only small changes in temperature because it is not influenced by these two types of coupling. In contrast, the temperature of CSTR 1 rises sharply when the thermal-mass coupling in opposite direction is switched on. In this type of coupling reactor 1 receives the cooling water from reactor 2, therefore, the coolant is preheated by reactor 2 so that its cooling power available for reactor 1 is lowered. Reactor 2 only shows minor changes in temperature. One can see that the calculations give the qualitatively correct results, i.e., one exclusively receives steady states as the results of different coupling modes and also the direction of the temperature changes is alway given correctly.

5.2.2. Coupling of Oscillatory States. The next experimental run shows the coupling of two oscillatory states (Figure 4b). In contrast to the model calculations, the states of the two reactors in the uncoupled case are not absolutely identical. This is due to small differences in the operation conditions of the two reactors which are unavoidable in the experiments, whereas in the calculations, the conditions are perfectly symmetric. If slightly asymmetric conditions are chosen in the simulations, similar differences in amplitudes, periods, and phase relations of the two reactors are found as in the experiments. However, the asymmetries do not cause any qualitative change in the behavior. According to the model calculations, oscillations are preserved in both reactors when thermal coupling or thermal-mass coupling in equal direction are investigated. Thermal coupling results in smaller oscillation amplitudes in reactor 2 but the mean value of the temperature of the oscillations is increased as it is predicted by the model calculations (Figure 4a). Thermal-mass coupling in equal direction also gives oscillations with diminished amplitudes in reactor 2 (compare with Figure 4a). For both types of coupling, the oscillations in reactor 2 are synchronized by the driving oscillations in reactor 1 in accordance with the model. The oscillation amplitudes of reactor 1 are smaller at the end of the experiment although thermal coupling and thermal-mass coupling in equal direction should not have any influence on reactor 1 (see model calculations in Figure 4a). This effect is due to a slight drop of the coolant flow rate in the experiment due to technical reasons when the coupling is activated. Figure 5b shows thermal-mass coupling in opposite direction starting with two oscillatory states. This type of coupling causes the oscillations in both reactors to vanish and to give way to steady states. This phenomenon is called phase death and is predicted by the calculation for this case of coupling. In the experiment, reactor 1 settles on a steady states at about $T_1 = 79$ °C ($T_1 = 77.0$ °C in the model), whereas reactor 2 cools to a low-temperature stationary solution of about $T_2 = 42$ °C ($T_2 = 42.3$ °C in the model). Mass coupling results in reestablished oscillations in reactor 1 because it is not influenced by the coupling. Reactor 2 shows a steady state ($T_2 = 41$ °C), whereas the calculations yield periodic oscillations, which are evidently too small in amplitude (2.6 °C) to be observed experimentally.

5.2.3. Coupling of Low-Temperature Steady States. Next, we use low-temperature steady states in both reactors for coupling ($T_1 = 44$ °C and $T_2 = 40$ °C for reactor 1 and reactor 2, respectively). For this type of coupling, the model calculations predict a high-temperature peak of reactor 2 after activation of thermal coupling (Figure 6a). Figure 6b shows the experimental thermal coupling of such steady states. After activation of the coupling, reactor 2 shows a very sharp temperature increase up to $T_2 = 89$ °C ($T_2 = 119.2$ °C in the model). The reaction in CSTR 2 becomes so vigorous that the evolving oxygen gas expels almost the whole reactor content through the reactor top (thermal runaway). The runaway initiates an emergency stop of the experiment, so that the behavior after the runaway cannot be compared with the corresponding calculation (Figure 6a) anymore. The reason for this behavior is the accumulation of unconverted hydrogen peroxide on the low-temperature branch of steady states. This accumulation is also a source of danger in the free running system.[29] Because the model calculations predict interesting behavior (rhythmogenesis) and show that only the transience to the final state should be dangerous, one has to use another strategy to perform this experiment. Guided by our calculations (Figure 7a) we switch off the feed of hydrogen peroxide solution of CSTR 2 as long as the coupling is switched off. When the coupling is turned on the dosing of hydrogen peroxide into reactor 2 is activated at the same time. Figure 7b shows the result. Indeed, the transience is much safer in accordance with the calculation because the first temperature peak after the coupling is now much lower ($T_2 = 66$ °C, $T_2 = 61.8$ °C in the model). Finally, oscillations are generated safely in reactor 2 (rhythmogenesis). Reactor 1 shows damped oscillations when thermal coupling is activated. Thermal coupling should not influence reactor 1 (see calculation in Figure 6a). In practice, however, we have a small influence on reactor 1 due to small changes in the coolant flow rate as it is explained above in the context of Figure 4b. Damped oscillations are generated in reactor 1 by the proximity of the Hopf bifurcation.

6. Discussion

In this work, we investigate the coupling of thermokinetic nonlinear systems experimentally as well as numerically. The main objective of the work is to verify in experiments the effects which the coupling of two thermokinetic reactors may have on the nonlinear behavior. There are theoretical studies about this topic in the literature, however, experimental investigations seem to be rare. On the other hand, the coupling of reactors by cooling circuits or in reactor cascades under stationary conditions is a standard procedure in technical applications. Therefore, the experimental investigation of the nonlinear behavior of coupled thermokinetic systems seems to be relevant for many applications in reaction engineering. We use four different types of coupling: thermal coupling, mass-coupling, thermal-mass coupling in equal direction, and thermal-mass coupling in opposite direction. All these coupling modes are studied in experiments. We investigate the dynamical effects which were introduced by the coupling. The model calculations predict that coupled oscillations can be converted to steady states (phase death) by thermal-mass coupling in opposite direction and that oscillations can be generated (rhythmogenesis) by thermal coupling of low temperature stationary solutions. Both effects can be found experimentally. The model calculations always give the correct results qualitatively. Often the coupling effects are predicted almost quantitatively, especially in the case of coupling oscillations or low-temperature steady states. The main differences between the experiment and the model are that the coolant flow $\dot{q}_{cool}$ has to be set to higher values as in the corresponding experiment to achieve comparable results for the uncoupled system, especially on the high-temperature branch of steady

states and inside the oscillatory region. Therefore, the bifurcation diagram of the model is shifted to higher coolant flows. These slight differences can be attributed to model imperfections, for example, the combination of several elementary steps to one reaction step in the model or inaccuracies of the kinetic constants.

The effects of mass coupling are overestimated by the model when high temperature steady states are coupled (compare Figure 3a and Figure 3b). On the branch of high temperature steady states, the temperature strongly depends on the coolant flow rate, so that small changes in the coolant flow have strong influence on the temperature and on the conversion of ethanol as well. Furthermore, the gas-phase is neglected in the calculations.[30] This neglection has the most pronounced consequences when high temperature steady states or oscillations with high amplitudes are involved (compare Figure 6a and Figure 6b). Moreover, the neglection of the heat loss inside the connection tube (residence time approximately 27 s for the feed flow $\dot{q}_f = 5.93$ L/h used) and the neglection of chemical reactions during this time are influencing the results. In the case of thermal coupling, no chemical reactions take place inside the coolant tube, and the effect of the neglected heat loss is lower as in the case of mass coupling since the flow rate of the coolant is in the range of $\dot{q}_{cool} = 20$ to 150 L/h corresponding to residence times of $\tau < 2$ s. We assume that these simplifications related with the coupling are of minor importance because the residence times mentioned above are small compared with the residence times of the reacting material inside the CSTRs ($\tau = 24$ min).

Besides the dynamics, aspects of safe reactor performance can be studied when nonisothermal systems are involved. Using this reaction process, great care must be taken, under which parameters the free running and the coupled system are operated. In the uncoupled system, educt accumulation on the low temperature branch of steady states can be critical. When coupling is activated one must also carefully check whether the final dynamics are uncritical but one also has to be sure the transients are safe. The model calculations can be used as a valuable guideline for finding safe coupling procedures. On the other hand, one might think about using these coupling modes to increase the yield of certain products, for example, the yield of the ethanal intermediate.

To summarize our results, the coupling of two reactors can change the dynamics of the reactor dramatically. In our experiments, we found that coupling can have a stabilizing effect as well as a destabilizing effect. These effects must be accounted for in the design of reactor networks.

Acknowledgment. The authors thank the German Bundesministerium für Bildung und Forschung for financial support (contract no. 03C0268B). We further thank our mechanic and electrician teams in Magdeburg and Stuttgart and our assisting students for their great effort.

References and Notes

(1) Marek, M.; Stuchl, I. *Biophys. Chem.* **1975**, *3*, 241. Fujii, H.; Sawada, Y. *J. Chem. Phys.* **1978**, *69*, 3830. Nakajima, K.; Sawada, Y. *J. Chem. Phys.* **1980**, *72*, 2231. Hauser, M. J. B.; Schneider, F. W. *J. Chem. Phys.* **1994**, *100*, 1058.

(2) Boukalouch, M.; Elezgaray, J.; Arneodo, A.; Boissonade, J.; DeKepper, P. *J. Phys. Chem.* **1987**, *91*, 5843.

(3) Bar-Eli, K.; Reuveni, S. *J. Phys. Chem.* **1985**, *89*, 1329.

(4) Doumbouya, S. I.; Münster, A. F.; Doona, C. J.; Schneider, F. W. *J. Phys. Chem.* **1993**, *97*, 1025.

(5) Laplante, J.-P.; Pemberton, M.; Hjelmfelt, A.; Ross, J. *J. Phys. Chem.* **1995**, *99*, 10 063.

(6) Stuchl, I.; Marek, M. *J. Chem. Phys.* **1982**, *77*, 2956.

(7) Laplante, J.-P.; Erneux, T. *J. Phys. Chem.* **1992**, *96*, 4931.

(8) Crowley, M. F.; Field, R. J. *J. Phys. Chem.* **1986**, *90*, 1907. Schneider, F. W.; Hauser, M. J. B.; Reising, J. *Ber. Bunsen-Ges. Phys. Chem.* **1993**, *97*, 55. Zeyer, K.-P.; Münster, A. F.; Hauser, M. J. B.; Schneider, F. W. *J. Chem. Phys.* **1994**, *101*, 5126.

(9) Dechert, G.; Zeyer, K.-P.; Lebender, D.; Schneider, F. W. *J. Phys. Chem.* **1996**, *100*, 19 043. Hohmann, W.; Kraus, M.; Schneider, F. W. *J. Phys. Chem.* **1999**, *103A*, 7606.

(10) Weiner, J.; Holz, R.; Schneider, F. W.; Bar-Eli, K. *J. Phys. Chem.* **1992**, *96*, 8915.

(11) van Heerden, C. *Chem. Eng. Sci.* **1958**, *8*, 133. Aris, R.; Amundson, N. R. *Chem. Eng. Sci.* **1958**, *7*, 121. Gilles, E. D.; Hofmann, H. *Chem. Eng. Sci.* **1961**, *15*, 328. Uppal, A.; Ray, W. H.; Poore, A. B. *Chem. Eng. Sci.* **1974**, *29*, 967. Sheplev, V. S.; Treskov, S. A.; Volokitin, E. P. *Chem. Eng. Sci.* **1998**, *53*, 3719.

(12) Jorgensen, D. V.; Aris, R. *Chem. Eng. Sci.* **1983**, *38*, 45.

(13) Kubíček, M.; Hofmann, H.; Hlaváček, V.; Sinkule, J. *Chem. Eng. Sci.* **1980**, *35*, 987.

(14) Svoronos, S.; Aris, R.; Stephanopoulos, G. *Chem. Eng. Sci.* **1982**, *37*, 357.

(15) Ravi Kumar, V.; Jayaraman, V. K.; Kulkarni, B. D.; Doraiswamy, L. K. *Chem. Eng. Sci.* **1983**, *38*, 673.

(16) Mankin, J. C.; Hudson, J. L. *Chem. Eng. Sci.* **1984**, *39*, 1807.

(17) Mankin, J. C.; Hudson, J. L. *Chem. Eng. Sci.* **1986**, *41*, 2651.

(18) Taylor, M. A.; Kevrikidis, I. G. *Chem. Eng. Sci.* **1993**, *48*, 2129.

(19) Brandes, H. In *Grundlagen der Chemischen Prozessregelung*; Oppelt, W., Wicke, E., Eds.; Oldenbourg: München, 1964; p 65. Hugo, P. *Proc. of the European Symp. on Chemical Reaction Engineering* **1968**, *4*, 459. Bush, S. F. *Proc. R. Soc.* **1969**, *309*, 1. Baccaro, G. P.; Gaitonde, N. Y.; Douglas, J. M. *AIChE J.* **1970**, *16*, 249. Beusch, H.; Fieguth, P.; Wicke, E. *Chemie-Ing.-Techn.* **1972**, *44*, 445. Schmitz, R. A.; Bautz, R. R.; Ray, W. H.; Uppal, A. *AIChE J.* **1979**, *25*, 289. Chang, M.; Schmitz, R. A. *Chem. Eng. Sci.* **1975**, *30*, 21. Heemskerk, A. H.; Dammers, W. R.; Fortuin, J. M. H. *Chem. Eng. Sci.* **1980**, *35*, 439. Wirges, H.-P. *Chem. Eng. Sci.* **1980**, *35*, 2141. Vleeschhouwer, P. H. M.; Fortuin, J. M. H. *AIChE J.* **1990**, *36*, 961. Haldar, R.; Phaneswara Rao, D. *Chem. Eng. Sci.* **1991**, *46*, 1197.

(20) Hafke, C.; Gilles, E. D. *Messen, Steuern, Regeln* **1968**, *11*, 204.

(21) Hafke, C. Dissertation, Universität Stuttgart, Germany, 1972.

(22) Steinbach, J. *Chemische Sicherheitstechnik*; VCH−Verlag: Weinheim, 1995; p 121.

(23) Dubil, H.; Gaube, J. *Chemie-Ing.-Techn.* **1973**, *8*, 529.

(24) Wittmer, P.; Ankel, T.; Gerrens, H.; Romeis, H. *Chemie-Ing.-Techn.* **1965**, *37*, 392.

(25) Ray, W. H.; Villa, C. M. *Chem. Eng. Sci.* **2000**, *55*, 275.

(26) Vleeschhouwer, P. H. M.; Garton, R. D.; Fortuin, J. M. H. *Chem. Eng. Sci.* **1992**, *47*, 2547.

(27) Grewer, T. *Thermal Hazards of Chemical Reactions*; Elsevier: Amsterdam, 1994; p 300.

(28) Morud, J. C.; Skogestad, S. *AIChE J.* **1998**, *44*, 888.

(29) Zeyer, K.-P.; Mangold, M.; Obertopp, T.; Gilles, E. D. *J. Phys. Chem.* **1999**, *103A*, 5515.

(30) Zeyer, K.-P.; Mangold, M.; Obertopp, T.; Gilles, E. D. *Chem. Eng. Sci.* **1999**, *54*, 4845.

(31) Zeyer, K.-P.; Pushpavanam, S.; Mangold, M.; Gilles, E. D. *Phys. Chem. Chem. Phys.* **2000**, *2*, 3605.

(32) Figgis, B. N.; Robertson, G. B. *Nature* **1965**, *205*, 694. Bond, A. M.; Clark, R. J. H.; Humphrey, D. G.; Panayiotopoulos, P.; Skelton, B. W.; White, A. H. *J. Chem. Soc., Dalton Trans.* **1998**, 1845.

(33) Verein Deutscher Ingenieure *VDI−Wärmeatlas, Berechnungsblätter für den Wärmeübergang*; VDI, GVC: Düsseldorf, 1994.

(34) Majer, C. *Parameterschätzung, Versuchsplanung und Trajektorienoptimierung für verfahrenstechnische Prozesse*; Dissertation; Universität Stuttgart, 1997.

(35) Alós, M. A.; Obertopp, T.; Mangold, M.; Gilles, E. D. *Praxis der Sicherheitstechnik* **1997**, *4*, 293.

(36) Mangold, M.; Kienle, A.; Gilles, E. D.; Mohl, K. D. *Chem. Eng. Sci.* **2000**, *55*, 441.

(37) Mansfield, J. M.; Pulley, R. A.; Wilson, J. A. *IChemE Research Event* **1995**, 484.